PROCEEDINGS OF SCIENCE

x

Higgs boson mass, width and CP measurements with the ATLAS detector

Firdaus Soberi[a,*] **on behalf of the ATLAS Collaboration**

[a] *University of Edinburgh, Edinburgh, United Kingdom*

E-mail: firdaus.soberi@cern.ch

The latest measurements of the Higgs boson mass, total width and CP properties with the ATLAS detector at the Large Hadron Collider are reviewed in this contribution. Using the combined Run1 and Run2 dataset, the mass is measured to be $m_H = 125.11 \pm 0.11$ GeV. The intrinsic width of the Higgs boson is constrained through indirect measurements in the combined off-shell and on-shell Higgs production channels. The current best value of the total width is $\Gamma_H = 4.3^{+2.6}_{-1.9}$ MeV at 68% confidence level coming from $H^* \to ZZ$ using a Neural Simulation-Based Inference technique. The Higgs CP properties are extensively studied and a pure CP-odd scenario is ruled out at more than 3σ level, although the CP-admixture scenario is still an open investigation. All results are consistent with the Standard Model. Future statistics and experiments are expected to bring down the uncertainties and further increase the precision of current measurements.

The XXXII International Workshop on Deep Inelastic Scattering and Related Subjects (DIS2025)
24-28 March 2025
Cape Town, South Africa

*Speaker

ISSN 1824-8039. Published by SISSA Medialab.

PoS(DIS2025)059

1. A "decade" after the Higgs discovery

The Higgs boson continues to be an important piece of the Standard Model more than a decade after its discovery [1–3]. Its quantum field coupling to fermions and bosons is crucial in explaining the origin of the mass for elementary particles. The shape of the Higgs potential and its connection to the electroweak vacuum is necessary in understanding the long-term stability of the Universe.

After its discovery and confirmation in Run1, the goal has since shifted to more precise measurements of its main properties, such as the mass, width, and the charge-parity (CP). As the Higgs boson is the only fundamental scalar field in the Standard Model, measuring its properties offers a unique opportunity to test current predictions and search for signs of new physics.

2. Higgs boson mass measurements

The mass of the Higgs boson, m_H, is a free parameter in the Standard Model. It must be measured experimentally since the mass determines many of the other Higgs properties such as the cross-sections, branching ratios and coupling strengths to other fundamental particles.

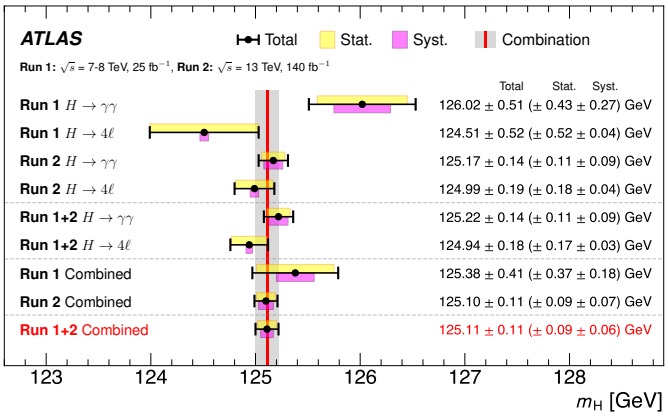

Figure 1: The measured Higgs boson mass from $H \to \gamma\gamma$ and $H \to ZZ^* \to 4\ell$ decay channels. The combined measured value in Run1 and Run2 is shown [4].

In the $H \to \gamma\gamma$ decay channel [5], the Higgs mass is extracted from the peak position of the di-photon invariant mass distribution, $m_{\gamma\gamma}$, minus the large continuum background, using a Double-Sided Crystal Ball function for the signal contribution. Compared to the previous measurement, the full Run2 analysis has a fourfold reduction in the dominant systematic (the photon energy scale and resolution), from 320 MeV to 80 MeV due to an improved photon clustering algorithm and photon energy scale calibration. The analysis was done using 14 categories split by: conversion type, projection of the di-photon transverse momentum onto the thrust-axis, $p_{Tt}^{\gamma\gamma}$, and the location of the two reconstructed energy clusters (central barrel, outer barrel or endcap). This reduced the total expected uncertainty by 3% from previous measurement using 101 event categories [6].

The $H \to ZZ^* \to 4\ell$ [7] is the golden channel with a clean peak over the ZZ^* background processes. The Higgs mass is extracted from the four-lepton invariant mass, $m_{4\ell}$, distribution using a profile likelihood fit in 4 categories ($2e2\mu, 2\mu2e, 4e, 4\mu$), based on the selected lepton leading and subleading pairs using the quadruplets from the identified Z-bosons. The full Run2 analysis has an improved signal to background discrimination using a deep neural network (DNN). The per-event resolution, σ_i, is estimated using a quantile-regression neural network output. An improved momentum-scale calibration, and electron calibration uncertainty correlation scheme, reduced the systematic uncertainty by 14%.

From the two channels in Figure 1, the $H \to \gamma\gamma$ channel is the most precise (δ_{m_H}=140 MeV) while $H \to ZZ^* \to 4\ell$ has a lower systematic uncertainty but is limited by statistics. The combined Run1 and Run2 measurement of m_H from the two channels reached a precision of 0.1% level:

$$m_H = 125.11 \pm 0.11\,\text{GeV}\ (0.09\ \text{stat}).$$

3. Higgs boson intrinsic width constraint

The Higgs boson's total decay width, Γ_H, is related to its lifetime and is the sum of its partial decay widths to all possible final states. Measuring the precise total width of the Higgs is crucial to check consistency with the Standard Model prediction. The predicted total width of 4.07 MeV for a 125 GeV Higgs [8] is too small to be directly measured at the LHC. The current experimental mass resolution in the high-resolution channels, such as $H \to \gamma\gamma$ and $H \to ZZ^* \to 4\ell$ is in the order of 1–2 GeV, i.e, several hundred times larger than the predicted width. Off-shell Higgs production offers an alternative route to measure the Higgs total width.

In the off-shell Higgs production, the interference between the different signal and background processes with same final states give rise to non-negligible cross section effects. The differential cross section of the invariant mass for a process that follows a Breit-Weigner distribution (e.g $gg \to H^* \to ZZ$) can be expressed as:

$$\frac{d\sigma_{gg\to H^*\to ZZ}}{dM^2_{ZZ}} = \frac{g^2_{ggH}\, g^2_{HZZ}}{(M^2_{ZZ} - m^2_H)^2 + m^2_H\Gamma^2_H} \tag{1}$$

In the denominator, the $m^2_H\Gamma^2_H$ term becomes insignificant in the off-shell limit (where $M^2_{ZZ} >> m^2_H$) while in the on-shell limit ($M^2_{ZZ} = m^2_H$) this term dominates. By manipulating the ratio of the off-shell to the on-shell cross sections, and the assumption that the couplings are equal in both cases, the ratio is proportional to the total width Γ_H times some phase-space constant. Through simultaneous binned likelihood fit, the ratio of the signal strength (linear scaling of the cross section to the one predicted by Standard Model) for the off-shell to the on-shell can be written as:

$$\mu_{\text{off-shell}}/\mu_{\text{on-shell}} = \Gamma_H/\Gamma^H_{SM} \tag{2}$$

The ATLAS experiment has constrained the total width of the Higgs in three separate main analyses, in $H^* \to ZZ(\to 4\ell, 2\ell 2\nu)$, $H^* \to WW \to e\nu\mu\nu$ and the $pp \to t\bar{t}H \to t\bar{t}t\bar{t}$ channel. In the $H^* \to ZZ$ analysis [9], the signal of the off-shell Higgs production shows up as a deficit in the $gg \to ZZ$ (gluon-gluon fusion, ggF), or the $q\bar{q} \to ZZ$ (quark-mediated electroweak, EW) production, due to negative interference between the off-shell Higgs and the continuum background processes. The $gg \to H^* \to ZZ$ interferes with the $gg \to ZZ$ continuum in the case of ggF processes. For the EW production, vector-boson fusion (VBF) and associated vector-boson production (VH) are considered as signals, while the continuum background comes from the vector-boson scattering process ($q\bar{q} \to ZZ + 2j$).

A full re-analysis for the 4ℓ was done with the Run2 dataset, but using a neural simulation-based inference (NSBI) technique [10] instead of the previously used neural network (NN) observables. Fourteen kinematic features are used including n_{jets}, $m_{4\ell}$ and m_{jj} to categorise the event. To select signal and control regions, a preselection discriminant, D_{pre}, is built from the combination of the signal and background scores of ggF and EW processes shown in Figure 2. The probability density ratio is estimated from a separate NN after the NSBI model is built from the kinematic features.

This NSBI technique improves upon previous measurement, since the previous analysis did not take into account the non-linearity (caused by large interference effects) in the signal strength, μ, which affects the probability density ratio estimate (causing potential bias in the extracted Γ_H).

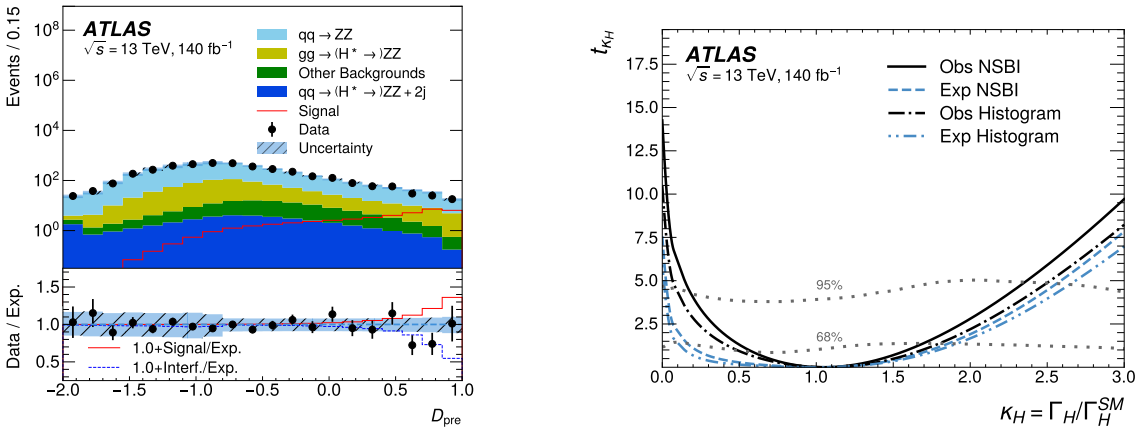

Figure 2: Off-shell $H^* \to ZZ$ measurement: (a) distribution of D_{pre} for various channels (b) values of the test statistic t_{κ_H} as a function of $t_{\kappa_H} = \Gamma_H/\Gamma_H^{SM}$, both NSBI and histogram-based fit using kinematic features are shown, with the black lines showing observed data and the dashed blue lines showing expected Asimov.

The evidence for off-shell Higgs production is observed with a significance of 3.7σ. Combined with the off-shell measurement $2\ell 2\nu$ and the same on-shell decay channels, the observed value of the Higgs total width is $\Gamma_H = 4.3^{+2.6}_{-1.9}$ MeV at 68% confidence level (CL), improved relative to the ATLAS previous result of $\Gamma_H = 4.4^{+3.1}_{-2.3}$ MeV using the same dataset, but without the NSBI method.

The $H^* \to WW$ analysis [11] has larger statistics than $H^* \to ZZ$, but is limited by systematics due to the missing transverse energy (MET) and high background contamination. A deep NN is used to classify the events and a proxy-variable to m_{WW} is used to enhance sensitivity with regard to the destructive interference regions. Combining with the on-shell Higgs results for the same final states gives an observed upper limit at 95% CL, for the rate of the off-shell Higgs boson production, at a value of 3.4 times the Standard Model prediction. This translates to an upper limit of 13.1 MeV for Γ_H. The third analysis exploits the four-top quark process observed in 2023 [12, 13]. The analysis was done using mainly the combined on-shell $t\bar{t}H$ (Higgs with association of top-quark pair) and the Higgs-mediated four tops $t\bar{t}t\bar{t}$ process with the off-shell Higgs production using $pp \to t\bar{t}t\bar{t}$. Combined with other on-shell Higgs measurement and doing likelihood ratio fit in the κ-framework, an upper limit of 450 MeV (160 MeV using constraint from κ_t considering loop-induced processes: ggF, $H \to \gamma\gamma$ and $H \to Z\gamma$) is set on the Γ_H at 95% CL.

4. Higgs boson CP properties

In the Standard Model, the Higgs boson is a scalar particle with even parity (spin-parity, J^P, of 0^+). This has been extensively measured since Run1 with pure states 0^-, $1^\pm$, $2^\pm$ excluded at more than 99% CL [14, 15]. Higgs boson is also predicted to be CP-even, which means it does not have a pseudoscalar (inverted parity) component. Signs of CP violation (existence of CP-odd component) would imply new physics and may partly explain the size of the matter-antimatter asymmetry (one of the Sakharov's conditions [16]). CP admixture between the CP-even and CP-odd components could be induced from anomalous couplings of the Higgs boson with the bosons or fermions such as the case of extended Higgs sector beyond Standard Model (BSM).

The Higgs boson interaction with fermions is possible at tree level through a modified Yukawa interaction:

$$\mathcal{L}_{Hff} = -\kappa_f \, y_f \, \bar{\psi}_f \, H(\cos\alpha + i\gamma_5 \sin\alpha) \, \psi_f \tag{3}$$

The CP-odd contribution is parameterised by the pseudoscalar term with α as the CP-mixing angle ($\alpha = 0$ reduces to the Standard Model scenario). ATLAS experiment has probed for CP-odd contribution in the fermionic sector through: Higgs-top targeting $t\bar{t}H$ production (in $H \to \gamma\gamma$ and $H \to b\bar{b}$ decay channels), Higgs-tau ($H \to \tau\tau$) and Higgs-gluon couplings ($H \to WW + 2j$).

The $t\bar{t}H$ production in $H \to \gamma\gamma$ decay [17] uses a boosted-decision tree (BDT) discriminant to reconstruct the top quark. The $t\bar{t}H$ production is observed at 5.2σ considering the CP-even hypothesis, and the pure-CP odd case ($\alpha = 90°$) is rejected at 3.9σ level. Values for CP-mixing angles $|\alpha| > 43°$ are excluded at 95% CL. For the $H \to b\bar{b}$ analysis [18], the CP-mixing angle is measured to be $\alpha = 11°^{+52°}_{-73°}$. The $H \to \tau\tau$ [19] was done in semi-leptonic or hadronic channels, with the signed acoplanarity angle ϕ^* between the tau decay planes as the CP-sensitive observable. A Recurrent Neural Network (RNN) is used to identify quark or gluon-initiated τ-jet candidates and BDT to reject τ from misidentified electrons. The CP-mixing angle is measured to be $\alpha = 9° \pm 16°$ at 68% CL, and the pure CP-odd hypothesis is rejected at 3.4σ.

Meanwhile, anomalous Higgs interaction with the gauge bosons can be modelled with the higher order SM effective field theory (SMEFT) operators. The operators can be represented in the Warsaw basis with dimension-6 Wilson coefficients, c_i, as the coupling modifier. ATLAS has probed the anomalous Higgs interaction with the vector bosons in HVV vertex (V=W,Z bosons) using VBF production channel in $H \to \gamma\gamma, H \to \tau\tau$ and $H \to ZZ^* \to 4\ell$ decays [20–22] with matrix element-based Optimal Observable (OO) as CP-sensitive variable:

$$OO_{\mathrm{CP}} = (2\,\mathrm{Re}\left[\mathcal{M}^*_{\mathrm{SM}}\,\mathcal{M}_{\mathrm{BSM}}\right])/|\mathcal{M}_{\mathrm{SM}}|^2 \tag{4}$$

For SM case with no CP-odd contribution, the OO shape is symmetric around 0. The limits in terms of the main 3 CP-odd Wilson coeeficients $c_{H\tilde{W}}$, $c_{H\tilde{B}}$ and $c_{H\tilde{W}B}$ are summarised in Figure 3. We can see that $c_{H\tilde{B}}$ and $c_{H\tilde{W}B}$ has $O(10)$ less sensitivity than $c_{H\tilde{W}}$.

The CP-odd contribution can also be studied using shape of the signed azimuthal angle difference. In $H \to WW + 2j$ analysis, both ggF+2j and VBF processes are considered. $\Delta\phi_{jj}$ is used as the CP-sensitive observable in which the CP-odd contribution introduces asymmetry to the otherwise symmetric $\Delta\phi_{jj}$ distribution. A recent study [23] explores possibility of using differential distribution from improved simplified template cross section (STXS) binning using 27 different categories. The results are interpreted in the SMEFT framework with CP-odd Wilson coefficients, $c_{H\tilde{G}}$ and $c_{H\tilde{W}}$, considered. $c_{H\tilde{W}}$ benefits from the STXS $\Delta\phi_{jj}$ bins with extra constraint coming from the Higgs transverse momentum cut, p_{T_H}.

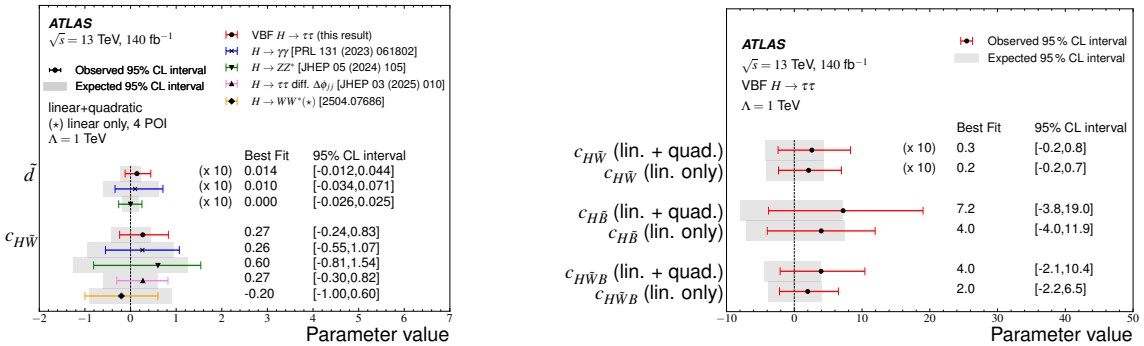

Figure 3: Wilson coefficients in SMEFT from multiple CP-odd measurements: (a) values for $c_{H\tilde{W}}$ in $H \to \gamma\gamma, H \to ZZ^*, H \to \tau\tau$ and $H \to WW^*$ (b) measured values of $c_{H\tilde{W}}$, $c_{H\tilde{B}}$ and $c_{H\tilde{W}B}$ with linear and linear+quadratic EFT order in $H \to \tau\tau$

The measured limits for the CP-odd Wilson coefficients ($c_{H\tilde{W}}$, $c_{H\tilde{B}}$, $c_{H\tilde{W}B}$ and $c_{H\tilde{G}}$) are consistent with the Standard Model prediction at 95% CL, for the BSM energy scale of $\Lambda = 1$ TeV.

5. Future Projections and Summary

Future colliders or upgrades offer powerful prospects to increase precision beyond the ones at LHC. The high luminosity LHC (HL-LHC) is projected to bring down the uncertainty in the Higgs mass to a level of about $\delta_{m_H} \sim 30$ MeV while lepton collider such as FCC-ee could bring this to $\delta_{m_H} \sim 4$ MeV [24]. The total Higgs width in the case of HL-LHC could have sub-MeV precision translating to around 17% accuracy and ultimately to 1% level with FCC-ee [24]. The other measurements such as CP properties could benefit from such improvements and the measured Wilson coefficients would be very important inputs towards EFT global fit effort.

In summary, the ATLAS experiment has measured the main properties of the Higgs boson to be consistent with the scalar particle predicted in the Standard Model. The mass measured with combined Run1 and Run2 data has a value of $m_H = 125.11 \pm 0.11$ GeV. The Higgs width is constrained (observed $\Gamma_H = 4.3^{+2.6}_{-1.9}$ MeV) using multiple indirect measurement of the off-shell Higgs and reaching to the level that is predicted by the Standard Model. The CP properties are consistent with the Standard Model and no sign of CP-violation is observed, leaving room for future measurements of Higgs CP-admixture. More studies are taking place with Run3 data, bringing larger statistics and better techniques along the way.

References

[1] ATLAS Collaboration, Physics Letters B **716** (2012) 1.
[2] CMS Collaboration, Physics Letters B **716** (2012) 30.
[3] ATLAS Collaboration, Nature **607** (2022) 52.
[4] ATLAS Collaboration, Phys. Rev. Lett. **131** (25 2023) 251802.
[5] ATLAS Collaboration, Physics Letters B **847** (2023) 138315.
[6] ATLAS Collaboration, Journal of High Energy Physics **2023** (2023) 88.
[7] ATLAS Collaboration, Physics Letters B **843** (2023) 137880.
[8] LHC Higgs Cross Section Working Group, CERN Yellow Rep. Monogr. **2** (2017) 1.
[9] ATLAS Collaboration, Physics Letters B **846** (2023) 138223.
[10] ATLAS Collaboration, Reports on Progress in Physics **88** (2025) 057803.
[11] ATLAS Collaboration, (2025), arXiv: 2504.07710 [hep-ex].
[12] ATLAS Collaboration, The European Physical Journal C **83** (2023) 496.
[13] ATLAS Collaboration, Physics Letters B **861** (2025) 139277.
[14] ATLAS Collaboration, Physics Letters B **726** (2013) 120.
[15] ATLAS Collaboration, The European Physical Journal C **75** (2015) 476.
[16] Andrei D Sakharov, Pisma Zh. Eksp. Teor. Fiz. **5** (1967) 32.
[17] ATLAS Collaboration, Phys. Rev. Lett. **125** (6 2020) 061802.
[18] ATLAS Collaboration, Physics Letters B **849** (2024) 138469.
[19] ATLAS Collaboration, The European Physical Journal C **83** (2023) 563.
[20] ATLAS Collaboration, Phys. Rev. Lett. **131** (6 2023) 061802.
[21] ATLAS Collaboration, Physics Letters B **805** (2020) 135426.
[22] ATLAS Collaboration, Journal of High Energy Physics **2024** (2024) 105.
[23] ATLAS Collaboration, (2025), arXiv: 2504.07686 [hep-ex].
[24] Sally Dawson et. al, (2022), arXiv: 2209.07510 [hep-ph].